International Journal of Engineering Science Invention (IJESI)
ISSN (Online): 2319-6734, ISSN (Print): 2319-6726
www.ijesi.org ||Volume 10 Issue 10 Series I || October 2021 || PP 37-42

Camera and LiDAR Calibration for Automating Electric Golf Cart

Haochen Yu[1], Arton Braimoviq[2], Su-chen Lin[2] , Qin Hu[2]
[1]*Electrical Engineering and Computer Science, University of Michigan, Ann Arbor, MI 48105, United States of America*
[2]*School of Engineering, Eastern Michigan University, Ypsilanti, MI 48197, United States of America*

ABSTRACT: *Sensor calibration is an important step in designing and building autonomous vehicles. In this paper, a novel pipeline for a successful LiDAR and Multiple Camera Calibration has been discussed. This method would shorten the time spent on performing sensor calibration, which was tested on an electric golf cart. A RGB camera and a LiDAR unit were used in this pipeline and the algorithm was implemented in Python language.*
KEYWORDS *— Autonomous golf cart, sensor calibration, LiDAR, cameras*

Date of Submission: 07-10-2021 Date of Acceptance: 21-10-2021

I. INTRODUCTION

The popularity of autonomous vehicle is rising in both academia and industry. Building a reliable Advanced Driver Assistance Systems (ADAS) in an effective way is challenging. In most ADAS systems, sensor calibration is a must step before further application such as sensor fusion, path planning, localization, object detection and tracking. The combination of RGB Cameras and LiDAR units is one of the most popular sensor-sets due to its capability of providing rich information from the environment. LiDAR provides three-dimensional point clouds while RGB cameras provide two-dimensional color images.

There are various methods for performing intrinsic and extrinsic calibration of cameras and LiDARs[1-5]. Researchers use chessboard and ArUco markers [6] for the calibration processes. This paper will discuss the detailed steps for calibrating cameras and LiDAR on a Club Car® Precedent electronic golf cart.

II. EXPERIMENTAL METHODS

2.1 Hardware System Design

The hardware set up of six cameras and one LiDAR on the Club Car® Precedent electronic golf cart is shown in Fig. 1. An ELP Megapixel Lens USB camera was mounted on the top front of a golf cart as shown in Fig. 1(a). The Velodyne VLP-16 LiDAR was mounted as well on the top of the golf cart behind the camera. Fig. 1(b) shows six cameras mounted on the golf cart to cover 360 degrees field of view. The LiDAR is positioned downward with an angle of 14^o to better detect pedestrians in front of the golf cart. The LiDAR has 16 channels, with 100 meters detection range.

(a) (b)

Figure 1: (a) LiDAR and camera set-up; (b) The golf cart with the LiDAR-camera set.

2. 2 Image Rectification

Images that are captured by an uncalibrated camera lens would have distortion caused by the physical shape of the lens [8]. There are two types of image distortions: tangential distortion and radial distortion. Tangential distortion occurs when the camera lens is not in parallel with the image plane. Radial distortion is caused by the physical shape of the camera lens. Scientist and researchers further classified radial distortion into two categories, the positive radial distortion (also known as barrel or fisheye distortion) [10,11], and negative radial distortion (also known as pincushion distortion). Barrel distortion as shown in Fig. 2, shows more distortion on corners than in center. Pincushion distortion, on the opposite of barrel distortion, shows larger magnification on the corners than in the center of an image. The cameras used in this study have barrel distortion.

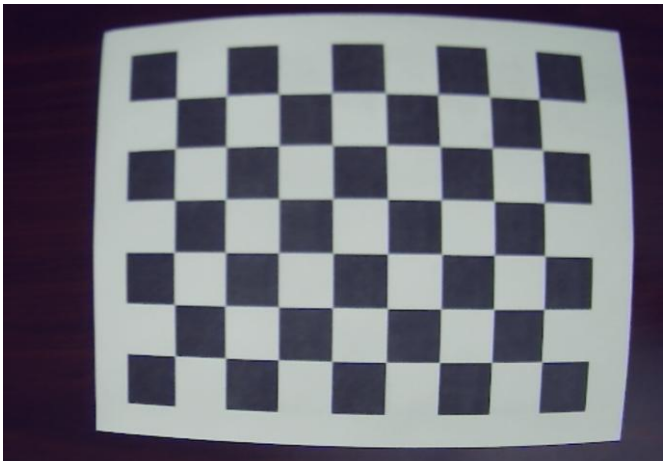

Figure 2: Example of barrel distortion.

To correct image distortions, a popular method used in OpenCV[8] is adopted here. In this method, five distortion coefficients, which are utilized to measure how much distortion an image has, need to be calculated. (x, y) are coordinates for any pixel in the original distorted image, while ($x_{corrected}$, $y_{corrected}$) are coordinates for the corrected image. The equations for the image rectification method are shown below:

$$x_{corrected} = x * (1 + k_1r^2 + k_2r^4 + k_3r^6) \quad (1)$$

$$y_{corrected} = y * (1 + k_1r^2 + k_2r^4 + k_3r^6) \quad (2)$$

$$x_{corrected} = x + [2p_1xy + p_2(r^2 + 2x^2)] \quad (3)$$

$$y_{corrected} = y + [p_1(r^2 + 2y^2) + 2p_2xy] \quad (4)$$

As shown in Equations (1-2) [8], k_1, k_2 *and* k_3 denotes for the radial distortion in x axis, y axis and z axis, and p1 and p2 describes the decentering distortion in x axis and y axis.

2.3 Intrinsic calibration

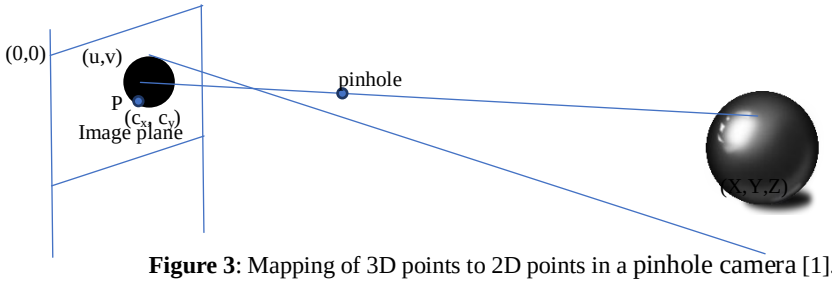

Figure 3: Mapping of 3D points to 2D points in a pinhole camera [1].

Fig. 3 shows a pinhole camera model, in which (X, Y, Z) represents a point of an object in the real world and (u, v) represents a pixel in the camera coordination system. Based on this model, the relationship between a 3D point in the world coordinates to a 2D point in an image coordinate is in Equation (5).

$$[\ u \quad v\ ]^T = K[\ R|T\ ][\ X \quad Y \quad Z\ ]^T \tag{5}$$

Here K is the camera matrix which is defined in Equation (6).

$$K = \begin{bmatrix} f_x & 0 & c_x \\ 0 & f_y & c_y \\ 0 & 0 & 1 \end{bmatrix} \tag{6}$$

In Equation (6), f_x and f_y denote the focal length in x axis and y axis, and c_x and c_y denote the offsets of principal points P from the corner of the image frame. R represent the rotation matrix which is defined in Equation (7) and T is the translation matrix which is defined in Equation (8).

$$R = \begin{bmatrix} r_{11} & r_{12} & r_{13} \\ r_{21} & r_{22} & r_{23} \\ r_{31} & r_{32} & r_{33} \end{bmatrix} \tag{7}$$

$$T = [t_x \quad t_y \quad t_z]^T \tag{8}$$

Equation 5 now can be re-written as below in Equation (9).

$$\begin{bmatrix} u \\ v \\ 1 \end{bmatrix} = \begin{bmatrix} f_x & 0 & c_x \\ 0 & f_y & c_y \\ 0 & 0 & 1 \end{bmatrix} \begin{bmatrix} r_{11} & r_{12} & r_{13} & t_x \\ r_{21} & r_{22} & r_{23} & t_y \\ r_{31} & r_{32} & r_{33} & t_z \end{bmatrix} \begin{bmatrix} X \\ Y \\ Z \\ 1 \end{bmatrix} \tag{9}$$

Here Equation (10) is also called projection matrix which is used to transform points from the world coordinates into an image coordinate system.

An 7x9 chessboard is used for the camera intrinsic calibration. During this process, multiple random coordinates were generated from the chessboard as shown in Fig. 4 (a)-(c). Corners of the chessboard were detected as shown in Fig. 4(d) first. Then the distortion coefficients and intrinsic matrix were calculated by python code under Robotic Operating System (ROS)[4,9]. Finally, a separate ROS program is used to process live image view from cameras and published to a rostopic for future processing.

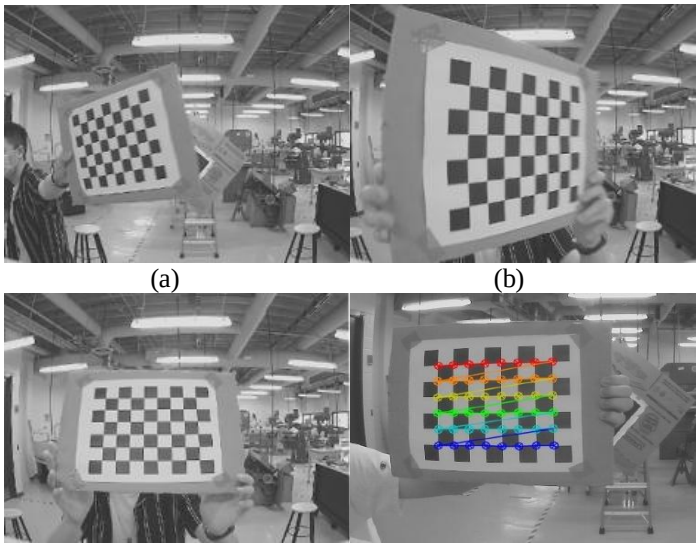

(a) (b)

(c) (d)

Figure 4: Chessboard used for calibration. (a)-(c) examples for chessboard at different view angles. (d) corner points are detected on the chessboard.

2.4 Extrinsic Calibration

To estimate the rotation matrix and translation matrix in Equation 9, two sets of 3D points were needed [7]. One set of them was from the LiDAR and another one from the camera. The LiDAR generates 3D points by default, but image sensors need to use the ArUco[3]markers to provide 3D information

As shown in Fig. 5(a), an ArUco marker contains black and white squares in a special encoded pattern to provide the depth information. ArUco markers are widely used in the Augmented Reality and Computer Vision applications [3]. A larger board with one ArUco marker printed on a cardboard is shown in Fig. 5(b).

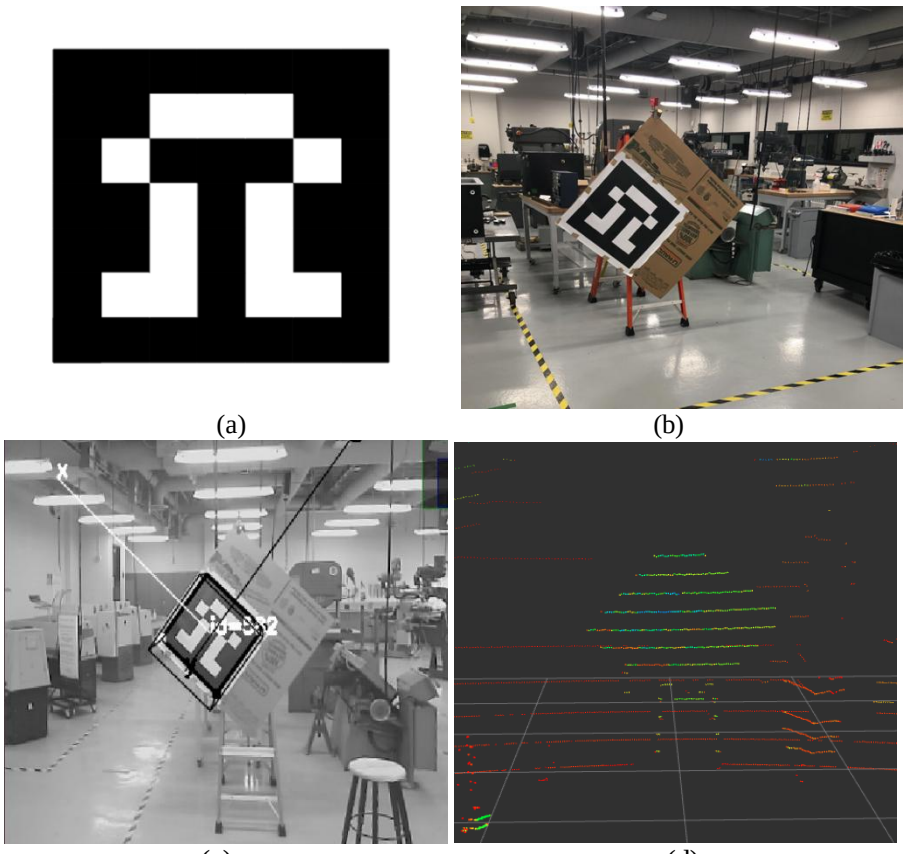

(a) (b)

(c) (d)

Figure 5: (a) An ArUco marker; (b) A cardboard with an ArUco marker; (c)3D coordinates of the cardboard; (d) LiDAR point cloud for the cardboard.

Fig. 5(c) shows an example of the 3D coordinates generated by using ArUco marker. The origin is the center of the ArUco marker, and the (x, y, z) represents the coordinates of the image plane. Each ArUco marker in the image has a unique ID. The LiDAR point cloud is collected manually in order to adjust the distance, and angle toward the LiDAR-camera set. A set of LiDAR point cloud for the ArUco board is shown in Fig. 5(d). Equation (10) was used to obtain the projection matrix between the LiDAR and the cameras.

III RESULTS AND DISCUSSION

To estimate the effectiveness of our approach, an experiment was conducted on an electric golf cart as shown in Fig. 2(b) with one RGB camera and one LiDAR unit mounted on it. In this study, three generic 1080P USB Megapixel Cameras and one Velodyne VLP-16 LiDAR unit were used.

To start the extrinsic calibration program, the projection matrix from the intrinsic calibration needed to be imported to the code first. The sides of the border S1 and S2, and b1, b2 and e for the ArUco marker were measured manually as shown in Fig 6(a). Other parameters that are necessary for running the extrinsic calibration code are: the number of the ArUco markers used, and the point cloud from the LiDAR.

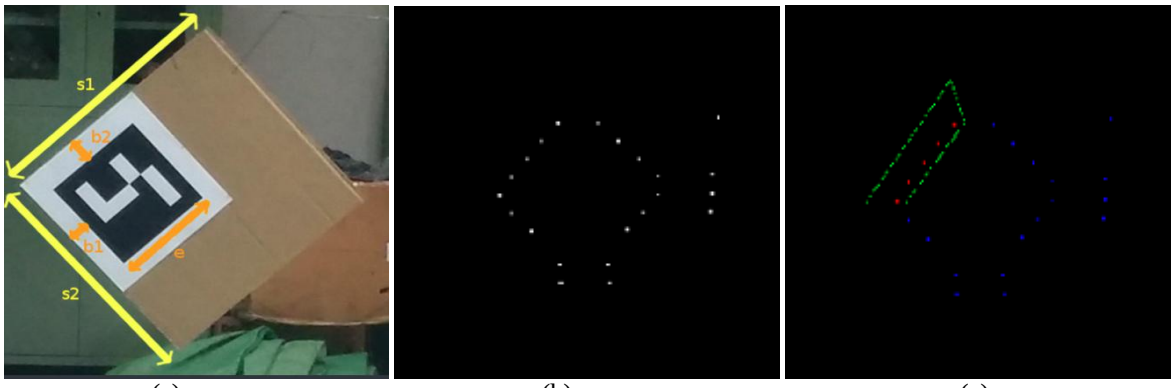

(a) (b) (c)

Figure 6: (a) A cardboard with an ArUco marker; (b) The edges of the cardboard detected; (c) A detected edge of the cardboard is circled.

Firstly, all four edges of the cardboard with an ArUco marker need to be detected as shown in Fig 6 (b). Then users need to manually draw a polygon around the dots that represents the four edges of the marker clockwise [5]. As shown in Fig 6(c), there were some noises if LiDAR detected other obstacles in the range. This will not affect the result since they would be excluded from the manually drawn polygons. The extrinsic calibration code eventually rendered both the rotation matrix and the translation matrix, which is shown in equation (10) and (11).

$$\begin{bmatrix} f_x & 0 & c_x \\ 0 & f_y & c_y \\ 0 & 0 & 1 \end{bmatrix} = \begin{bmatrix} 526.7884350 & 0.0000000 & 277.178380 \\ 0.00000000 & 526.781239 & 268.660230 \\ 0.00000000 & 0.00000000 & 1.0000000 \end{bmatrix} \tag{10}$$

$$\begin{bmatrix} r_{11} & r_{12} & r_{13} & t_x \\ r_{21} & r_{22} & r_{23} & t_y \\ r_{31} & r_{32} & r_{33} & t_z \end{bmatrix} = \begin{bmatrix} -0.585801 & -0.806058 & 0.0843055 & 0.616382 \\ -0.415017 & 0.209001 & -0.885483 & -2.3716 \\ 0.69613 & 0.209001 & -0.456961 & 0.88083 \end{bmatrix} \tag{11}$$

IV. CONCLUSION

In conclusion, a sensor calibration method was implemented on an electric golf cart. The calibration process includes intrinsic and extrinsic calibrations. Image rectification is also discussed as a pre-treatment to camera images. Three cameras and one LiDAR unit were successfully calibrated. This would build a foundation for the LiDAR-camera set to gain the necessary information about surroundings around the golf cart accurately and conveniently.

ACKNOWLEDGEMENT

The authors would like to acknowledge John Earl, and the Autonomous Golf Cart (AGC) project group at EMU for their gracious support and work. In addition, we would like to acknowledge the EMU Game Above College of Engineering and Technology's financial support of this summer project.

REFERENCES

[1]. Y. Li et al., "Application of 3D-LiDAR & Camera Extrinsic Calibration in Urban Rail Transit," 2020 IEEE 5th International Conference on Intelligent Transportation Engineering (ICITE), 2020, pp. 456-460, doi: 10.1109/ICITE50838.2020.9231446.

[2]. Y. Lyu, L. Bai, M. Elhousni and X. Huang, "An Interactive LiDAR to Camera Calibration," 2019 IEEE High Performance Extreme Computing Conference (HPEC), 2019, pp. 1-6, doi: 10.1109/HPEC.2019.8916441.

[3]. P. Huang, W. Hong, H. Chien and C. Chen, "Extrinsic calibration of a multi-beam LiDAR system with improved intrinsic laser parameters using v-shaped planes and infrared images," IVMSP 2013, 2013, pp. 1-4, doi: 10.1109/IVMSPW.2013.6611921.

[4]. Z. Zhang, "A flexible new technique for camera calibration" IEEE Transactions on Pattern Analysis and Machine Intelligence, vol. 22, no. 11, pp. 1330-1334, Nov. 2000, doi: 10.1109/34.888718.

[5]. A. Dhall, K. Chelani, V. Radhakrishnan, K.M. Krishna, LiDAR camera calibration using 3D-3D point correspondences, Cornell University, Ithaca, NY, 2017.

[6]. Y. Wang, Z. Zheng, Z. Su, G. Yang, Z. Wang and Y. Luo, "An Improved ArUco Marker for Monocular Vision Ranging," 2020 Chinese Control And Decision Conference (CCDC), 2020, pp. 2915-2919, doi: 10.1109/CCDC49329.2020.9164176.

[7]. F. Itami and T. Yamazaki, "An Improved Method for the Calibration of a 2-D LiDAR With Respect to a Camera by Using a Checkerboard Target," in IEEE Sensors Journal, vol. 20, no. 14, pp. 7906-7917, 15 July15, 2020, doi: 10.1109/JSEN.2020.2980871.

[8]. K. Lelowicz, "Camera model for lens with strong distortion in automotive application," 2019 24th International Conference on Methods and Models in Automation and Robotics (MMAR), 2019, pp. 314-319, doi: 10.1109/MMAR.2019.8864659.

[9]. S. Rivera, A. K. Iannillo, S. Lagraa, C. Joly and R. State, "ROS-FM: Fast Monitoring for the Robotic Operating System(ROS)," 2020 25th International Conference on Engineering of Complex Computer Systems (ICECCS), 2020, pp. 187-196, doi: 10.1109/ICECCS51672.2020.00029.

[10]. J. Kannala and S. S. Brandt, "A generic camera model and calibration method for conventional, wide-angle, and fish-eye lenses," in IEEE Transactions on Pattern Analysis and Machine Intelligence, vol. 28, no. 8, pp. 1335-1340, Aug. 2006, doi: 10.1109/TPAMI.2006.153.

[11]. M. Lee, H. Kim and J. Paik, "Correction of Barrel Distortion in Fisheye Lens Images Using Image-Based Estimation of Distortion Parameters," in IEEE Access, vol. 7, pp. 45723-45733, 2019, doi: 10.1109/ACCESS.2019.2908451.

Haochen Yu, et. al. "Camera and LiDAR Calibration for Automating Electric Golf Cart." *International Journal of Engineering Science Invention (IJESI)*, Vol. 10(10), 2021, PP 37-42. Journal DOI- 10.35629/6734